NEURAL REGENERATION RESEARCH
January 2017, Volume 12, Issue 1
www.nrronline.org

RESEARCH ARTICLE

# Real-time and wearable functional electrical stimulation system for volitional hand motor function control using the electromyography bridge method

**Hai-peng Wang**[1], **Zheng-yang Bi**[2], **Yang Zhou**[1], **Yu-xuan Zhou**[2], **Zhi-gong Wang**[1, 3, *], **Xiao-ying Lv**[2, 3]
1 Institute of RF- & OE-ICs, Southeast University, Nanjing, Jiangsu Province, China
2 State Key Lab of Bioelectronics, Southeast University, Nanjing, Jiangsu Province, China
3 Co-innovation Center of Neuroregeneration, Nantong University, Nantong, Jiangsu Province, China

***How to cite this article:*** *Wang HP, Bi ZY, Zhou Y, Zhou YX, Wang ZG, Lv XY (2017) Real-time and wearable functional electrical stimulation system for volitional hand motor function control using the electromyography bridge method. Neural Regen Res 12(1):133-142.*

***Funding:*** *This work was supported by the National Natural Science Foundation of China, No. 90307013, 90707005, 61534003; a grant from the Science & Technology Pillar Program of Jiangsu Province in China, No. BE2013706.*

## Graphical Abstract

**A novel prototype system of volitional hand motor function rebuilding system for paralysis rehabilitation: real-time and wearable "electromyography bridge"**

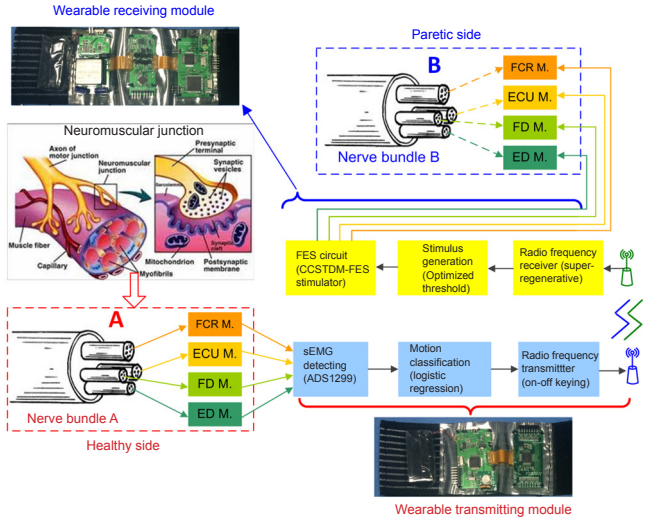


***Correspondence to:***
*Zhi-gong Wang, Dr.-Ing., zgwang@seu.edu.cn.*

***orcid:***
*0000-0002-9203-4683 (Zhi-gong Wang)*

***doi:*** *10.4103/1673-5374.197139*

***Accepted:*** *2016-11-10*

## Abstract

Voluntary participation of hemiplegic patients is crucial for functional electrical stimulation therapy. A wearable functional electrical stimulation system has been proposed for real-time volitional hand motor function control using the electromyography bridge method. Through a series of novel design concepts, including the integration of a detecting circuit and an analog-to-digital converter, a miniaturized functional electrical stimulation circuit technique, a low-power super-regeneration chip for wireless receiving, and two wearable armbands, a prototype system has been established with reduced size, power, and overall cost. Based on wrist joint torque reproduction and classification experiments performed on six healthy subjects, the optimized surface electromyography thresholds and trained logistic regression classifier parameters were statistically chosen to establish wrist and hand motion control with high accuracy. Test results showed that wrist flexion/extension, hand grasp, and finger extension could be reproduced with high accuracy and low latency. This system can build a bridge of information transmission between healthy limbs and paralyzed limbs, effectively improve voluntary participation of hemiplegic patients, and elevate efficiency of rehabilitation training.

***Key Words:*** *nerve regeneration; functional electrical stimulation; logistic regression; rehabilitation of upper-limb hemiplegia; electromyography control; wearable device; stroke; frequency-modulation stimulation; hand motion; circuit and system; real-time; neural regeneration*

## Introduction

Functional electrical stimulation (FES) has been introduced as a neurorehabilitation method to artificially activate sensory and motor systems following central nervous system disease or injury, such as spinal cord injury and stroke (Popović, 2014; Shen et al., 2016; Wade and Gorgey, 2016). The first noninvasive FES system was used for foot drop correction of hemiplegic patients by Liberson et al. (1961). Many novel FES systems have been designed as surface or implantable stimulation systems for controlling arms and hands (Saxena et al., 1995; Ijzerman et al., 1996; Kilgore et al., 1997; Knutson et al., 2012; Hara et al., 2013).

The NESS Handmaster (Ijzerman et al., 1996) and the FES system (Nathan, 1989) belong to the push-button controlled FES method (or switch-based FES). Both of these methods use on/off stimulation with pre-programmed sequences to help spinal cord injury patients recover hand grasp movements and other daily functions. Electromyography (EMG) has been used for on/off control in EMG-triggered FES (Cauraugh et al., 2005) or proportional EMG-controlled FES (Saxena et al., 1995; Thorsen et al., 2001; Hara et al., 2013) and capitalizes on the principle of intension-driven motion. Therapeutic effects were reduced by approximately half if FES was applied without voluntary recipient involvement (Barsi et al., 2008). Preliminary results (McGie et al., 2015) suggest that motor-evoked potential of brain computer interface-controlled FES (Pfurtscheller et al., 2003) and EMG-controlled FES can elicit greater neuroplastic changes than conventional therapy. However, EMG-controlled FES requires some residual movement of the affected arm or hand, so it is not applicable with severely disabled stroke survivors. Contralaterally controlled FES is a promising therapy designed to improve recovery of paretic limbs after stroke. Two case series pilot studies (Knutson et al., 2009, 2014) and an early-phase randomized controlled trial (Knutson et al., 2012) verified the efficiency of contralaterally controlled FES. However, it is important for the success of FES therapy to include the contralateral limb in volitional control of electrically induced contraction in the affected limb.

Based on the success of volitional control of FES, our group previously designed an FES system for restoring motor function in post-stroke hemiplegic patients (Huang et al., 2014). In that system, a frequency-modulation stimulation algorithm based on surface EMG (sEMG) and the support vector machine model were used. However, sEMG thresholds need to be carefully chosen and force reproduction performance has not yet been established. The system is also too difficult to wear and remove.

The specific objectives of this paper were: (1) to use statistical experiments and analyses to optimize the primary parameter "sEMG thresholds" of the frequency-modulation stimulation generation algorithm formerly proposed by our group and to verify the force reproduction performance; (2) to develop a low-complexity algorithm based on logistic regression for hand movement classification achieved by these sEMG thresholds; (3) to develop a wireless and wearable FES system using the EMG-bridge method for real-time volitional hand motor function control, and to assess the feasibility of this system in real-time control of four hand movements. This novel system is a wearable EMG-bridge system that is distributed *via* a contralateral sEMG-controlled FES system providing more convenience to use at home. The size, power, and overall cost have been significantly reduced compared with the previous prototype (Huang et al., 2014).

## Subjects and Methods

### Wearable EMG-bridge system overview

The concept of the EMG-bridge method was that each target muscle of the paralyzed limb had its own source muscle in the healthy controller limb, and the sEMG signals of the muscles were transformed by stimulation pulses that could be adjusted by modulating the pulse frequency. Additionally, the mimicked real-time activation state of the corresponding source agonist muscles could be realized in the paralyzed limb.

The block diagram of the wearable EMG-bridge system for volitional hand motor function control is shown in **Figure 1**. This system included a wearable transmitting module and a wearable receiving module. The transmitting module consisted of a sEMG signal detecting circuit, an analog-to-digital converter, a microcontroller unit (MCU), and a radio frequency transmitter. The receiving module consisted of a radio frequency receiver, an MCU, and an FES circuit. The upper-extremity sEMG signals were recorded by the sEMG detecting circuit. The signals were then converted to digital signals through the analog-to-digital converter under control of the MCU in the wearable transmitting module. In this MCU, the digital signal process, which included filtering and amplifying, was initially performed, then a classification algorithm was used to determine upper-limb movement status. Simultaneously, according to the distinguished motion state, the sEMG signal of the chosen channel was encoded using the algorithm for generating the stimulating pulse. The coded signals containing information for the selected output stimulation were wirelessly transmitted to the receiving module under control of the MCU in the transmitting module. The signals were then sent to the MCU for decoding. The trigger pulses were generated by the decoder in the MCU, which then triggered the FES circuit to generate output high-voltage, biphasic, and charge-balanced stimulating pulses. The transmitting module was worn on the volitional controlling upper extremity and the receiving module was attached to the controlled limb.

### System hardware description

An analog front-end ADS1299 (Texas Instruments Inc., Dallas, TX, USA) with single-differential sEMG sensors was selected to integrate the sEMG signal detecting circuit and analog-to-digital converter. The ADS1299 had eight low-noise programmable gain amplifiers and eight 24-bit analog-to-digital converters, which could support a maximum of eight channel sEMG signal acquisitions. After sending the digitalized sEMG signals to the MCU, they were band-pass filtered from 20 to 500 Hz and amplified with a gain of 1,000.

A fully integrated super-regenerative receiver chip operating in the 335/433 MHz band was selected as the radio frequency receiver for its simplicity and efficiency in low-power and short-range communication, as previously described by our group (Wang et al., 2012) and realized in a 0.35-μm complementary metal oxide semiconductor process. Similarly, an on-off keying circuit with an operating frequency that matched the radio frequency receiver was used as the radio frequency transmitter.

The mixed signal MCU MSP430F169 (Texas Instruments Inc.) served as the processor. This low-powered MCU is especially suited for design in wearable systems. The connection interface between the ADS1299 and processor in the wearable transmitting module comprised a serial peripheral interface and general purpose input/output. The MCUs in the wearable transmitting module and in the wearable receiving module were exchanged with their data through the general purpose input/output with the radio frequency transmitter and receiver, with a data rate of 2 kbps.

The FES circuit was based on the complementary current source and time division multiplexing as previously discussed (Wang et al., 2015). This pulse-triggered FES stimulator includes a low-powered MCU of type STM32F103 (ST-Microelectronics Inc.) with an ARM Cortex™-M3 core, a stimulation driving stage, a biphasic and time division multiplexing output circuit, and a high-voltage power supply.

**Optimization of sEMG thresholds**

The choice of sEMG thresholds for stimulating pulse generation algorithm is crucial in the EMG-bridge system, because the sEMG thresholds are not only used for motion classification, but also for modulation of stimulation frequency. For stimulation pattern generation in our work, we used an EMG-controlled stimulation algorithm based on a previously described threshold (Huang et al., 2014). EMG activity recorded from the able-bodied limb was used as a template for electrical stimulation to elicit upper-limb movement. The stimulation frequency was simultaneously modulated by the preset EMG signal threshold and refractory period of muscle stimulation (minimal interval between two neighboring pulses) (Zhou et al., 2011). The EMG activity was mapped into a stimulation pattern that modulated muscle output by varying the frequency. The force reproduction performance of this stimulation strategy correlated with the EMG signal threshold, although it remains to be shown whether the voluntary muscle force can be reproduced with high fidelity. In our study, we implemented the torque reproduction test, which used this stimulation strategy with different thresholds. The experimental procedure of the force tracing test was similar to a previously described study (Zhou et al., 2016). The threshold was optimized by repeatable force reproduction experiments in a number of subjects and was finally programmed in the prototype system to increase the convenience of use. Additionally, compared with previous studies using a separate stationary or a transient contraction for sEMG recognition (Lorrain et al., 2011), our system concurrently employed these two situations.

**Subjects**

All volunteers were recruited by posting posters on billboards at Southeast University of China. Six healthy subjects (five males and one female; 26.3 ± 2.9 years of age) participated in the study. Each subject was asked to refrain from strenuous exercise of the upper extremities for at least 24 hours before the study. All subjects provided written informed consent before participation, and this study was approved by the Human Subjects Review Board of Southeast University.

**Experiment protocol 1: Torque reproduction test**

The main target muscles in this test were the flexor carpi radialis muscle and extensor carpi ulnaris muscle. Isometric wrist joint torque was acquired using a custom-made device (Zhou et al., 2016). The sEMG and torque signals were sampled with a 16-bit analog-to-digital converter acquisition board PCI-6220 (National Instruments Inc., Austin, TX, USA) at a frequency of 1 kHz. A self-designed PC-based software was used to record data for off-line analysis and provided visual feedback to the subject.

The flowchart and waveforms of each step in the wrist joint torque reproduction test are shown in **Figure 2**. Initially sEMG signals and isometric wrist joint torque were recorded during a voluntary test motion composed of three repetitions with varying force outputs (**Figure 2a**, **b**). In every wrist flexion/extension repetition, the subject was instructed to perform a wrist torque from 0 Nm to 30% maximal voluntary contraction, then to relax to 0 Nm. The duration of each cycle was 20 seconds (slow trail) and 10 seconds (fast trial). For each sEMG signal channel, the threshold ($Thr_k$) was set and the value was determined as follows:

$$MAV_k = \frac{1}{N}\sum_{i=1}^{N}\left|x_k^{(i)}\right| \quad (1)$$

$$Thr_k = N_k \cdot MAV_k \quad (2)$$

In Equation (1), $MAV_k$ represents the mean absolute value of sEMG data ($\bar{x}(i)$) in the kth channel for 2-second contraction movement (Phinyomark et al., 2012), and $Thr_k$ was acquired using the ratio parameter $N_k$ as presented in Equation (2).

According to the signal noise ratio of the acquired sEMG and Equation (1) and (2), three sEMG thresholds were selected with a ratio of 60%, 90%, and 120% of the mean absolute value, which means that $N_k$ equaled 0.6, 0.9, and 1.2. The mean absolute value was calculated based on three 5-second segments of sEMG extracted from the voluntary test motion, which elicited 30% maximal voluntary contraction. Afterwards, the stimulating pulse trains of varying frequency were generated from the sEMG signals with different thresholds, and this step was conducted using Matlab 2014 software (MathWorks Inc., Natick, MA, USA) on a personal computer with an Intel CPU (Core i3, 2.3-GHz) and 6-GB memory (**Figure 2c**). The generated stimulating pulse trains were then stored in the MCU flash memory of the wearable receiving module. The MCU delivered the trigger pulses to

the FES circuit in a real-time manner with a time window of 1 ms. The receiving module was used to stimulate the flexor carpi radialis/extensor carpi ulnaris muscles, and the corresponding stimulated torque signals were recorded (**Figure 2d**) to determine the optimized sEMG threshold. The stimulation procedure in each subject was also conducted at least 24 hours after the previous steps. The stimulating current used in the experiment was adjusted to induce a 30% maximal voluntary contraction of wrist motion using a simulating pulse train (500 μs, 50 Hz).

Three metrics were used to quantify the stimulated force reproduction performance (Zhou et al., 2016): Pearson correlation coefficient (*R*) was defined as the similarity between the stimulated and the origin torque. *Root mean square error (RMSE)* was the absolute difference between two cases. *Mean bias error (MBE)* represented the average bias of reproduced torque from the voluntary torque, and was defined as:

$$MBE = \frac{1}{M}\sum_{i=1}^{M}(|Tv_i| - |Ts_i|) \quad (3)$$

where *T*v represented voluntary torque and *T*s represented stimulated torque.

Logistic regression for hand motion classification: four classes of hand motions, plus the no-motion class were investigated in this study, because they were the most commonly employed upper-limb motions in clinical rehabilitation studies (Li et al., 2010; Knutson et al., 2012; Craven et al., 2015). The five classes were: wrist extension, wrist flexion, finger extension, hand grasp, and no motion. It is important to note that the above-described motions were two degrees of freedom, while the logistic regression algorithm was used for one degree of freedom motion classification and control. Therefore, the other one degree of freedom motion and control could only be realized by changing the detecting and stimulating electrodes. Thus, sEMG data for logistic regression classifier training and testing were described as follows: (1) wrist motion data were acquired, and two sEMG data channels were detected using bipolar surface Ag/AgCl ECG electrodes (Junkang Medical Supplies., Shanghai, China) that were spaced 2 cm apart. These were placed on the forearm above the wrist flexor (flexor carpi radialis) and extensor (extensor carpi ulnaris), and a reference electrode was placed on the lecranon. (2) Two sEMG data channels that correlated with hand motions were similarly collected, with electrodes placed on the finger flexor (flexor digitorum) and extensor (extensor digitorum). (3) Data were obtained from six healthy subjects; each was asked to perform three repetitions of each dynamic motion class for a 2-second contraction with up-ramping force exertion and a 2-second relaxation. The first two data sets were used for training and the last set was used for testing. Data were also sampled by ADS1299 in the EMG-bridge system at a rate of 1 kHz and were digitally filtered at 20–500 Hz, with a digital gain of 1,000.

In this logistic regression classifier, the voltage amplitude of the sEMG signal was selected as the feature. For each motion class, the feature set was constructed on each of the two channels, which satisfied the following equations:

$$\vec{x}^{(i)} = [x_{\mathrm{Ch1}}^{(i)}, x_{\mathrm{Ch2}}^{(i)}] \in \{feature_{\mathrm{g}}\},\ \mathrm{g}=1,2,3,4; \quad (4)$$

$$\text{if}\quad x_{\mathrm{Ch1}}^{(i)} > \mathrm{Thr}_{\mathrm{Ch1}} \quad \text{or} \quad x_{\mathrm{Ch2}}^{(i)} > \mathrm{Thr}_{\mathrm{Ch2}}$$

$$y^{(i)} = \begin{cases} 0, & \text{if} \quad \mathrm{g}=1,3 \\ 1, & \text{if} \quad \mathrm{g}=2,4 \end{cases} \quad (5)$$

$x^{(i)}$ represented the $i_{\mathrm{th}}$ sampled sEMG signal amplitude data vector containing channel Ch1 and Ch2, $y^{(i)}$ represented each motion result. Then, the suitable data ($x^{(i)}$, $y^{(i)}$) was collected into the corresponding supervised feature set and fed into the classifier. The remaining data were labelled as no-motion class. The hypothesis function $h_\theta(x)$ and cost function $J(\theta)$ of the logistic regression were calculated as follows:

$$h_\theta(\vec{x}) = \frac{1}{1+e^{-\theta\vec{x}^T}},\quad \theta = [\theta_1, \theta_2] \quad (6)$$

$$J(\theta) = \frac{1}{m}\sum_{i=1}^{m}[-y^{(i)}\log(h_\theta(\vec{x}^{(i)})) - (1-y^{(i)})\log(1-h_\theta(\vec{x}^{(i)}))] \quad (7)$$

The parameter $\theta$ could be solved by a gradient descent of $J(\theta)$ with the training data. In the testing phase, the classification result ($d^{(j)}$) was obtained by Equation (8) when the testing data were fed into the classifier. For example, 'Ch1_muscle' meant that the recognized movement was related to the agonist motion muscle where CH1 electrodes placed.

$$d^{(j)} = \begin{cases} \mathrm{Ch1\_muscle}, & \text{if} \quad x_{\mathrm{Ch2}}^{(j)} < (-\theta_1/\theta_2)\, x_{\mathrm{Ch1}}^{(j)} \\ \mathrm{Ch2\_muscle}, & \text{if} \quad x_{\mathrm{Ch2}}^{(j)} > (-\theta_1/\theta_2)\, x_{\mathrm{Ch1}}^{(j)} \end{cases} \quad (8)$$

**Experiment protocol 2: Motion classification off-line test**

The data sets from the four motion classes were collected from all six subjects as described above. To pre-verify the logistic regression classifier performance in the real-time EMG-bridge system, the mean optimized sEMG thresholds acquired from the above torque reproduction test of six subjects were used for the wrist flexion/extension and hand grasp/finger extension classifications. The performance of the trained classifier in identifying a movement was measured by *classification accuracy (CA)*, which was defined as the number of correctly classified samples divided by the total number of testing samples (Li et al., 2010). The logistic regression classifier parameters ($\theta$) were averaged over data sets of all subjects to calculate the overall CA. The off-line analysis was conducted using Matlab 2014 software.

Wearable design and implementation: Photographs of the wearable EMG-bridge system prototype are shown in **Figure 3**. The wearable transmitting module and the wearable receiving module were both fixed with a stretchable armband for ease of wear. The maximum stretchable length of the armband was 30 cm, which was maintained to adapt to the upper extremity of most individuals (22–28 cm). Additionally, a soft anti-static film was tailored and assembled to the top of the armband to prevent electrostatic interference. In the wearable transmitting module, there were two primary printed circuit boards consisting of an ADS1299 printed circuit board and a controller-printed circuit board. The sizes of the two printed circuit boards were 30 × 60 × 10 $mm^3$ and

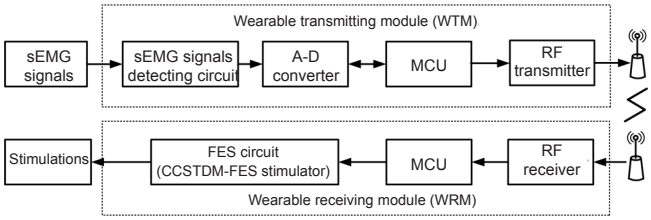


**Figure 1 Block diagram of the wearable EMG-bridge system for volitional hand motor function control.**
sEMG: Surface electromyography; MCU: microcontroller unit; RF: radio frequency; FES: functional electrical stimulation; CCSTDM: complementary current source and time division multiplexing; A-D converter: analog-to-digital converter.

$25 \times 60 \times 10$ mm$^3$, respectively. In the wearable receiving module, there were three main printed circuit boards that included a high-voltage power-printed circuit board, a FES circuit-printed circuit board and a controller-printed circuit board, which were all fixed with equal distance between to the armband. The dimension of each printed circuit board was $30 \times 60 \times 10$ mm$^3$, $25 \times 60 \times 10$ mm$^3$, and $30 \times 60 \times 10$ mm$^3$. Two 32-cm custom-made cables based on the flexible-printed circuit were used to connect the three circuit boards. The wearable transmitting module and the wearable receiving module were supplied by a 12-V and 500-mAh rechargeable Li-battery. Simultaneously, the radio frequency transmitter and receiver-printed circuit boards were a miniaturized design with an area of $2.5 \times 3$ cm$^2$ and $1.3 \times 1.1$ cm$^2$. **Figure 3B** shows the receiver-printed circuit board with an 8-pin packaged super-regenerative receiver chip, and the photomicrograph of this chip in the 0.35-μm complementary metal oxide semiconductor is presented in **Figure 3C**. The area of the chip was $550 \times 775$ μm$^2$, and the maximum data rate was 20 kbps.

### Experiment protocol 3: Real-time sEMG bridging test

The mean optimized sEMG thresholds and the averaged trained logistic regression classifier metrics ($\theta$) in the off-line test were used for the real-time volitional sEMG bridging motion control test. The six healthy subjects were randomly divided into three experimental pairs. To simulate the stroke patient using the proposed EMG-bridge system, two subjects acted as the role of the controller and the controlled within each pair, and then these roles were exchanged for another repetition. For each controller, the wearable transmitting module was worn on the right forearm, and for each controlled subject, the wearable receiving module was applied in the same position. The real-time bridging test consisted of two procedures. The first step was real-time wrist flexion/extension control, and the second was for the hand grasp/finger extension control.

A customized hand motion tracking system based on the Leap Motion sensor (Leap Ltd., San Francisco, CA, USA) and PC software (Visual C#) was developed for measuring wrist and finger joint angles in the controlling and controlled limbs. In our tracking system, the measured wrist joint angle was defined as the angle between hand and forearm. The five-finger joint angle was represented as the mean metacarpophalangeal joint (MPJ) angles of the five fingers (5F-MPJ). Three metrics were used to quantify real-time performance. The *normalized cross-correlation* ($\rho_{xy}$) was defined as the similarity, synchronism, or functional coupling of three measured angle trajectories, which was calculated as:

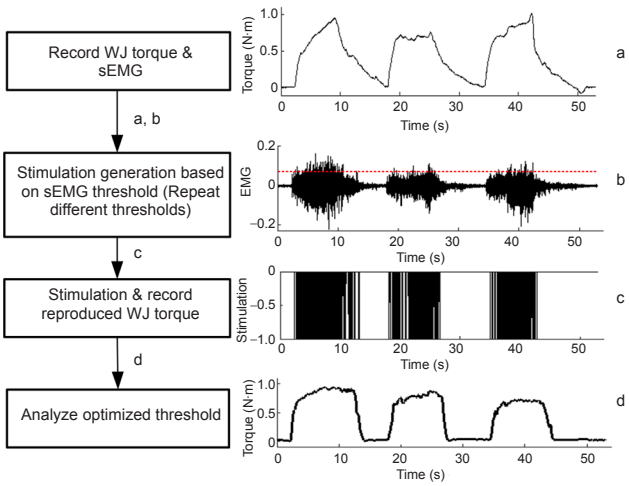


**Figure 2 Flowchart of the wrist joint torque reproduction test using stimulating pulse generation algorithm based on the sEMG threshold.**
(a) Recorded isometric voluntary wrist joint torque signal waveform (slow trial, wrist flexion movement); (b) recorded voluntary sEMG signal waveform; (c) generated stimulation waveform using algorithm based on different thresholds; (d) recorded stimulated wrist joint torque. WJ: Wrist joint; sEMG: surface electromyography; s: second.

$$\rho_{xy} = \frac{\left(\sum_{n=-\infty}^{+\infty} x(n)y(n+m)\right)^2}{\sum_{n=-\infty}^{+\infty} x^2(n) \cdot \sum_{n=-\infty}^{+\infty} y^2(n)} \quad (9)$$

where $x(n)$ and $y(n)$ were the joint angle trajectories of the controller and the controlled, respectively. The variable $m$ correlated with the metric *delay time* ($T_d$), which was the time offset of the controlled trajectory compared with the controlling trajectory. The last metric *motion completion rate (MCR)* was defined as the percentage of successfully completed motions.

### Statistical analysis

Statistical analysis was performed using SPSS statistics 19.0 software (IBM corp., Chicago, IL, USA) and the paired Wilcoxon signed-rank test. The results are expressed as the mean ± SD. $P \leq 0.05$ was considered significantly different.

## Results

### Selection of three sEMG thresholds from the torque reproduction test results

**Table 1** shows some initial parameters from the wrist joint torque reproduction test, including mean absolute sEMG values that corresponded with the four wrist test behaviors (slow/fast wrist extension and slow/fast wrist flexion), and the stimulation current intensity for the six subjects. **Figure 4** presents voluntary and stimulated wrist torque trajectories using the stimulating pulse generation algorithm with three

different ratios ($N_k$ = 60%, 90%, and 120%) of sEMG mean absolute values in each test behavior as the threshold. The representative trajectories were acquired from subject B for illustration.

The assessing metrics (*R*, *RMSE*, and *MBE*) for each movement trial using the stimulation generation algorithm with three different ratios are presented in **Figure 5**. The mean *R* value across the six subjects and four behaviors was 0.80 ± 0.07 for TH_60% protocol ($N_k$ = 60%), 0.84 ± 0.08 for TH_90% protocol ($N_k$ = 90%), and 0.86 ± 0.08 for TH_120% protocol ($N_k$ = 120%). The corresponding average *RMSE* values were 20.7 ± 4.8%, 20.1 ± 4.6%, and 21.1 ± 6.0%, respectively. The corresponding average MBE values were 0.02 ± 0.10, 0.07 ± 0.08, and 0.10 ± 0.08, respectively. Additionally, the TH_90% protocol showed significantly higher *R* values for wrist flexion behaviors ($Z$ = 2.201, $P$ = 0.028) and fast wrist extension ($Z$ = 2.023, $P$ = 0.043) than the TH_60% protocol, and slightly (not significantly) higher *R* values than the TH_60% protocol for the slow wrist extension. The TH_120% protocol showed significantly higher R values for the slow wrist extension ($Z$ = 2.201, $P$ = 0.028), fast wrist extension ($Z$ = 2.023, $P$ = 0.043), and fast wrist flexion ($Z$ = 1.992, $P$ = 0.046) compared with the TH_60% protocol, and slightly higher *R* values than the TH_60% protocol for wrist flexion with slow trail (**Figure 5A**). For the four-type wrist behaviors, no significant differences were found in *RMSE* values between the three protocols, with the exception that the *RMSE* value obtained for the fast wrist flexion movement generated using the TH_60% protocol was significantly lower than in the TH_90% protocol ($Z$ = 1.992, $P$ = 0.046) (**Figure 5B**). Simultaneously, the MBE result for the TH_120% protocol showed significantly higher negative offset from the target torque ($P$ < 0.05), which indicated that the TH_120% protocol did not produce sufficient torque to trace the target compared with the TH_60% protocol (**Figure 5C**). Although the TH_120% protocol also showed a slightly higher bias from the target, and considering the trade-off between the similarity and offset with the target force, the TH_90% protocol was selected as the threshold-definition method for the stimulation generation and classification.

### Motion classification off-line test result in subjects with the optimized sEMG threshold and logistic regression classifier

According to the torque reproduction test above, the mean thresholds were computed across the six subjects as 0.030 V for wrist movements. The hand motion thresholds were also defined as 90% of the sEMG mean absolute value, but without force tracing test. The mean thresholds for the hand grasp/finger extension were 0.105 V and 0.130 V, respectively. **Table 2** presents the trained logistic regression classifier parameter ($-\theta_1/-\theta_2$) and the corresponding performance metric CA in the off-line analysis. Then, the average parameter ($-\theta_1/-\theta_2$) across the six subjects was selected as the trained logistic regression classifier, and the total CA for all datasets from the six subjects was analyzed off-line. **Figure 6** illustrates the scatter plot of the sEMG signals of two channels and decision boundary using the trained logistic regression classifier with optimized $\theta$ and the above-defined thresholds. The *CA* of the wrist flexion/extension across the total six subjects was 99.92% using the parameter ($-\theta_1/\theta_2$=1.05), and the *CA* of the hand grasp/finger extension was 98.90% using the parameter ($-\theta_1/\theta_2$=1.01).

### Real-time sEMG bridging test results in subjects with the wearable functional electrical stimulation system

The sEMG signals and stimulation pulses from two channels in the real-time bridging test with the wearable EMG-bridge system were measured using an oscilloscope (DSO7034A; Agilent Inc., CA, USA). The representative waveforms are presented in **Figure 7**. The task was the wrist flexion/extension control test, and the controller was subject B. To illustrate the bridging mechanism, the acquired digital sEMG data were converted to waveforms using the digital-to-analog converter from the MCU in the wearable receiving module. Additionally, the stimulating current intensity was 7.25 mA for flexion movement and 8.6 mA for extension movement, which provided the mean intensities across six subjects described in the torque reproduction test. **Figure 8** illustrates the normalized wrist joint and 5F-MPJ joint tracing trajectories from a pair of subjects acting as the controller and the controlled, respectively. The *maximum cross-correlation* ($\rho_{xy}$) was 0.918 for wrist joint tracing and 0.829 for 5F-MPJ tracing, while the *delay time* ($T_d$) was 0.1 second for wrist joint tracing and 0.15 second for 4F-MPJ tracing. **Table 3** presents three metrics ($\rho_{xy}$, $T_d$, and *MCR*), which were used to assess the real-time bridging tracing test performed in six subjects. The mean ± SD of maximum $\rho_{xy}$ between the paired trajectories was 0.77 ± 0.10 for wrist joint tracing and 0.78 ± 0.08 for 5F-MPJ tracing, respectively. The mean ± SD of $T_d$ was 142 ± 132 ms for wrist joint tracing and 392 ± 188 ms for 5F-MPJ tracing, respectively. Additionally, the mean ± SD of *MCR* in wrist movements was 97.87 ± 2.59%, and the MCR in hand motions was 95.18 ± 2.80%.

## Discussion

We present a novel sEMG-controlled FES system, which can enhance volitional hand motor function control of FES induced muscle contractions during different target movements. The method presents two advantages over previous systems. (1) After statistically analyzing and selecting an optimized sEMG amplitude threshold from six healthy subjects, the low-complexity algorithm was based on logistic regression for hand movement classification, which allowed for more accuracy and reliability compared with the multi-channel system. (2) Using a series of novel design concepts, including the integration of a detecting circuit and analog-to-digital converter, a miniaturized FES circuit technique, a low-power super-regeneration chip for wireless receiving, and two wearable armbands, we were able to create a prototype system that was significantly reduced in size, power, and overall cost, making it wearable and suitable for rehabilitation at home. Simultane-

**Table 1 Subject parameters of wrist joint in torque reproduction test**

| | Subjects[a] | | | | | | |
|---|---|---|---|---|---|---|---|
| Motion | A | B | C | D | E | F | Average |
| WES_MAV[b] (V) | 0.0255 | 0.0359 | 0.0284 | 0.0313 | 0.0414 | 0.0394 | 0.0337 |
| WEF_MAV[c] (V) | 0.0244 | 0.0331 | 0.0264 | 0.0286 | 0.0396 | 0.0375 | 0.0316 |
| WFS_MAV[d] (V) | 0.0430 | 0.0206 | 0.0278 | 0.0340 | 0.0435 | 0.0298 | 0.0331 |
| WFF_MAV[e] (V) | 0.0325 | 0.0183 | 0.0245 | 0.0266 | 0.0461 | 0.0329 | 0.0302 |
| WE_Intensity[f] (mA) | 9 | 9 | 7 | 10 | 7.5 | 9 | 8.6 |
| WF_Intensity[g] (mA) | 8.5 | 8 | 8 | 7 | 6 | 6 | 7.25 |

[a]Subjects A–F; [b]WES_MAV, [c]WEF_MAV, [d]WFS_MAV, and [e]WFF_MAV represent the mean absolute values (MAVs) of sEMG signals that correspond with the four wrist test behaviors, including slow/fast wrist extension (WES/WEF), and slow/fast wrist flexion (WFS/WFF). Each MAV was calculated based on three 5-second segments of sEMG extracted from each voluntary test behavior that elicited a 30% maximal voluntary contraction. The sEMGs were acquired from wrist extensor (slow trial), wrist extensor (fast trial), wrist flexor (slow trial), and wrist flexor (fast trial), separately. [f]WE_Intensity and [g]WF_Intensity represent stimulation intensity of wrist extension and flexion task, respectively.

**Table 3 Measured metrics of the real-time bridging test using the wearable EMG-bridge system**

| Subject pair (controller ->controlled) | *max* ($\rho_{xy}$[a]) (WJ[d]) | $T_d$[b] (ms) (WJ) | *MCR*[c] (%) (WJ) | *max* ($\rho_{xy}$) (5F-MPJ[e]) | $T_d$ (ms) (5F-MPJ) | *MCR* (%) (5F-MPJ) |
|---|---|---|---|---|---|---|
| A–> B | 0.92 | 100 | 97.76 | 0.83 | 100 | 95.12 |
| B–> A | 0.77 | 400 | 100.00 | 0.82 | 450 | 93.33 |
| C–> D | 0.86 | 150 | 95.00 | 0.85 | 500 | 95.24 |
| D–> C | 0.72 | 50 | 100.00 | 0.83 | 350 | 100.00 |
| E–> F | 0.71 | 50 | 100.00 | 0.74 | 300 | 95.74 |
| F–> E | 0.66 | 100 | 94.44 | 0.63 | 650 | 91.67 |
| Mean ± SD | 0.77±0.10 | 142±132 | 97.87±2.59 | 0.78±0.08 | 392±188 | 95.18±2.80 |

[a]$\rho_{xy}$: Normalized cross-correlation of two measured angle trajectories, which was calculated as Equation (9). [b]$T_d$: Delay time offset of the controlled trajectory compared with the controlling trajectory. [c]*MCR*: Motion completion rate, which is defined as the percentage of successfully completed motions. [d]WJ: Wrist joint angle, which is defined as the angle between hand and forearm. [e]5F-MPJ: Mean metacarpophalangeal joint angles from the five fingers.

**Table 2 Parameter of classifier & performance metrics for motion classification off-line analysis**

| Subject | $-\theta_1/\theta_2$ (wrist) | CA[b] (%) (wrist) | $-\theta_1/\theta_2$ (hand) | CA (%) (hand) |
|---|---|---|---|---|
| A | 0.975 | 100.00 | 1.072 | 99.73 |
| B | 0.926 | 100.00 | 0.926 | 99.35 |
| C | 1.100 | 99.60 | 1.008 | 100.00 |
| D | 1.200 | 99.70 | 1.043 | 96.35 |
| E | 1.025 | 99.96 | 1.080 | 99.96 |
| F | 1.052 | 100.00 | 0.949 | 100.00 |
| Optimized $\theta$[a] | 1.050 | 99.92 | 1.010 | 98.90 |

[a]Optimized $\theta$ means using the average parameter ($-\theta_1/\theta_2$) across six subjects as the trained logistic regression classifier and analysis of total classification accuracy (CA) for all datasets from six subjects. [b]CA represents motion classification accuracy of the off-line trained classifier.

ously, the adoption of a Li-battery as a power supply helped to ensure greater safety of use (Cook et al., 2015).

This proposed wearable EMG-bridge system helped to overcome the limitations of previous systems (Huang et al., 2014) that had many wires and were cumbersome to wear. It is also interesting that this system can be used in a healthy subject without the use of a ground ring (Huang et al., 2014). The subject can successfully control contralateral wrist and fingers through the use of a wearable transmitting module worn on the upper extremity and a wearable receiving module applied to the other limb, as previously described (Knutson et al., 2012). This was mainly possible because of the contribution of the CCTDM-FES circuit design (Wang et al., 2015), which used the multiplexer circuit to quickly establish a short connection between two stimulating electrodes and reduce the impact of the stimulation artifact. Therefore, it could be applied to upper-extremity hemiplegia to assist with rehabilitation at home, if positioning of the electrodes on the skin can be properly made (Knutson et al., 2012). Stroke patients do not typically require stimulation to the wrist (or finger) flexor, so this system could assist patients in the stimulation of the wrist (or finger) extensor by changing the electrode positions according to markings and photos.

Nevertheless, there are still several aspects worth noting from this study:

(1) Because the above experiments were performed on healthy subjects and not impaired subjects after stroke, the musculoskeletal physiology is different between healthy and impaired subjects with stroke or spinal cord injury (Hafer-Macko et al., 2008; Biering-Sørensen et al., 2009), so we cannot completely infer feasibility of this proposed wearable EMG-bridge system. However, we believe that it can provide excellent performance for contralaterally controlled FES applications (Knutson et al., 2014), because the healthy side of a patient with upper-extremity hemiplegia is similar to

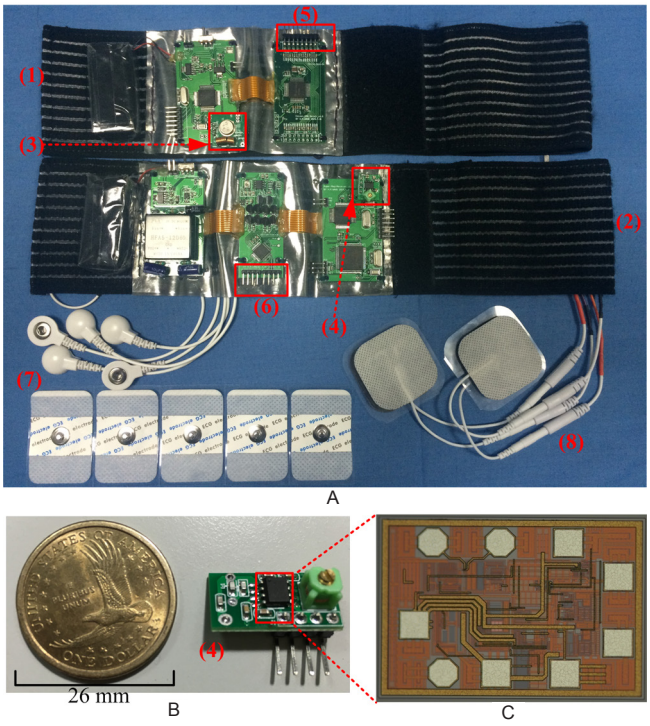


**Figure 3 Prototype wearable EMG-bridge system.**
(A) The prototype wearable EMG-bridge system. (B) The radio frequency receiver board. (C) The self-designed integrated super-regenerative receiver chip in 0.35-mm complementary metal oxide semiconductor. (1) Transmitting wearable band; (2) receiving wearable band; (3) on-off keying circuit (radio frequency transmitter); (4) super-regenerative receiver circuit (radio frequency receiver); (5) interface between sEMG electrodes and sEMG signal detecting circuit; (6) interface between functional electrical stimulation circuit and gelled stimulation electrodes; (7) surface Ag/AgCl electrocardiogram electrodes for sEMG signal acquisitions; (8) gelled stimulation electrodes ($4 \times 4$ cm$^2$). sEMG: Surface electromyography.

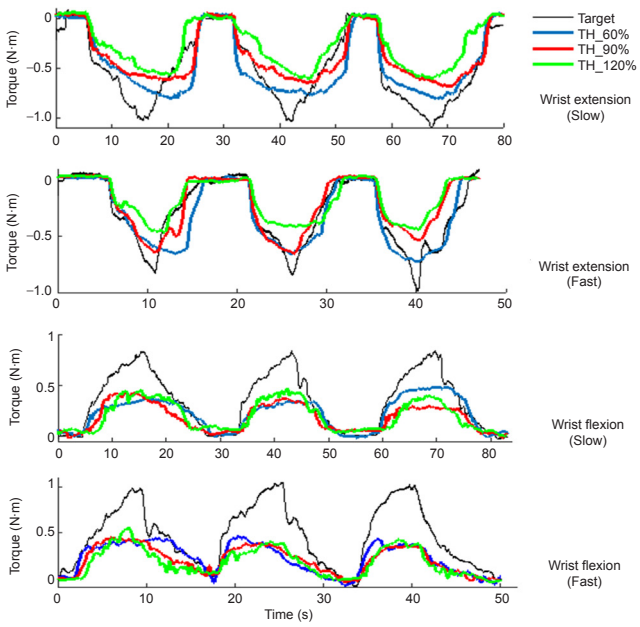


**Figure 4 Representative wrist torque trajectories of voluntary and stimulated using stimulation generation algorithms by selecting three ratios ($N_k$ = 60%, 90%, and 120%) of surface electromyography mean absolute value in each movement trial for the thresholds (Subject B).**
Four isometric wrist movements from top to bottom involved slow extension, fast extension, slow flexion, and fast flexion. In each panel, the original torque tracks of voluntary motion, and the torque elicited by the algorithm based on three different thresholds, are presented in black, blue, red, and green, respectively.

healthy subjects. Further clinical research should be conducted in various patients to test the robustness of the wearable EMG-bridge system.

(2) According to results from the above-described wrist joint torque reproduction test, the stimulating pulse generation algorithm we used could result in the stimulated force tracing the voluntary force to a certain degree. However, at the force peak point shown in **Figure 4**, it significantly deteriorated performance. During voluntary contractions, the central nervous system modulates muscle force by adjusting the number of recruited motor units (recruitment coding) and the activation frequency (rate coding) (Kamen and Du, 1999). Analogously in the FES, the stimulation intensity (amplitude and pulse width) and frequency can be modulated to control the muscle force. Kesar et al. (2008) reported that frequency modulation showed better performance for both peak forces and force-time integrals in response to the fatiguing trains than pulse duration modulation, while producing similar levels of muscle fatigue. Therefore, the frequency modulation was selected for our stimulating pulse generation algorithm, but the frequency modulation with fixed intensity was responsible for the deterioration in force tracing performance, which is in accordance with previous results (Binder-Macleod and McDermond, 1992) showing that varying any stimulation parameters independently results in a nonlinear force response. Additionally, both recruitment and rate coding strategies more effectively prevent fatigue than the use of independent modulation alone (Johnson and Fuglevand, 2011). A pulse width and frequency co-modulation stimulation strategy based on sEMG time-domain features was recently proposed by our group (Zhou et al., 2016). Although the co-modulation strategy exhibited better voluntary force reproduction and more fatigue resistance than the traditional sEMG proportional control strategy, the high complexity of computation and transplantation to the wearable system requires further development.

(3) In our current system, only one agonist muscle corresponding with specific movement was chosen, whereas in reality, the smooth, continuous, and functional voluntary movement was performed by the agonist, stabilizer, and synergist together. Additionally, the most typical need for stroke survivors is finger and thumb extension, rather than wrist extension. Therefore, methods such as non-negative matrix factorization (Jiang et al., 2009, 2014) for extracting time-invariant synergies in multi-channel sEMG and multi-pad electrode surface stimulation system (Malešević et al., 2012; Popović-Maneski et al., 2013) are needed to realize multi-degree of freedom bridging-control movements.

In summary, the present study proposed a wearable EMG-bridge system for real-time volitional hand motor function

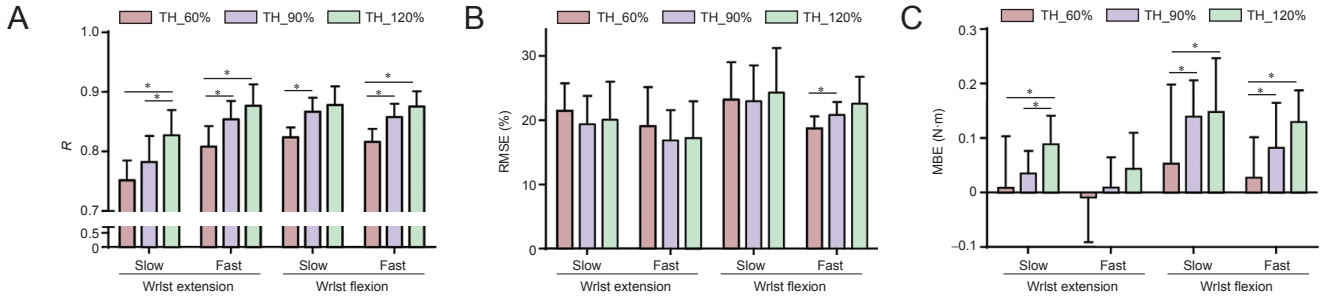


**Figure 5 Three metrics (R, RMSE, and MBE) values for the three different thresholds of isometric wrist torque reproduction test.**
(A) Pearson correlation coefficient (*R*); (B) root mean square error (RMSE); (C) mean bias error (MBE). The results are shown as the mean ± SD ($n$ = 6). *$P \leq 0.05$, as determined by paired Wilcoxon signed-rank test.

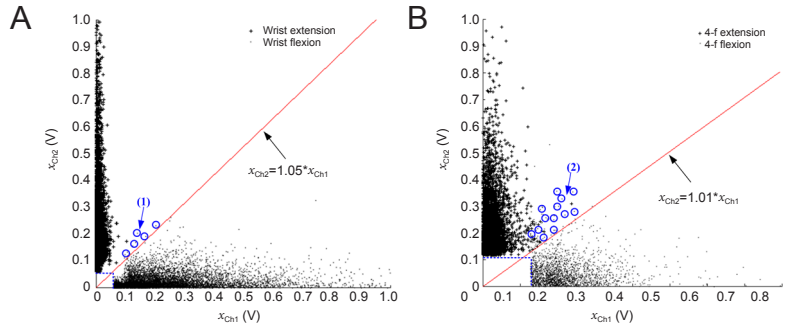


**Figure 6 Scatter plot of the two channels surface electromyography signals and decision boundary using the trained logistic regression classifier with optimized $\theta$ and thresholds ($N_k$ = 90%) for off-line motion classification performed on datasets from six subjects.**
(A) Wrist flexion and extension ($-\theta_1/\theta_2$ = 1.05). (B) Grasp and finger extension ($-\theta_1/\theta_2$ = 1.01). (1) and (2) are the error classification results using logistic regression classifier.

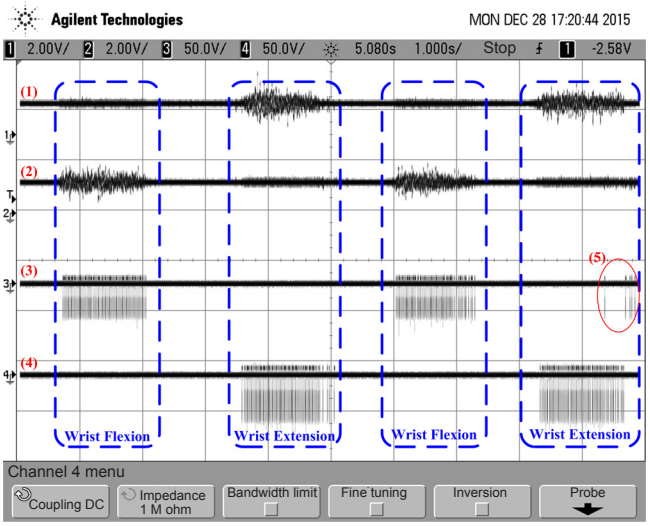


**Figure 7 Representative measured waveforms of signals in the real-time bridging test using the wearable EMG-bridge system.**
Surface EMG was acquired from subject B and the loaded resistors between the stimulation terminals were 10 kΩ. (1) and (2) were surface EMG signals detected from the wrist flexor and wrist extensor, respectively. (3) and (4) were $Ch_1$ outputs (stimulation to the wrist flexor) and $Ch_2$ outputs (stimulation to the wrist extensor) in the functional electrical stimulation circuit, respectively. EMG: Electromyography.

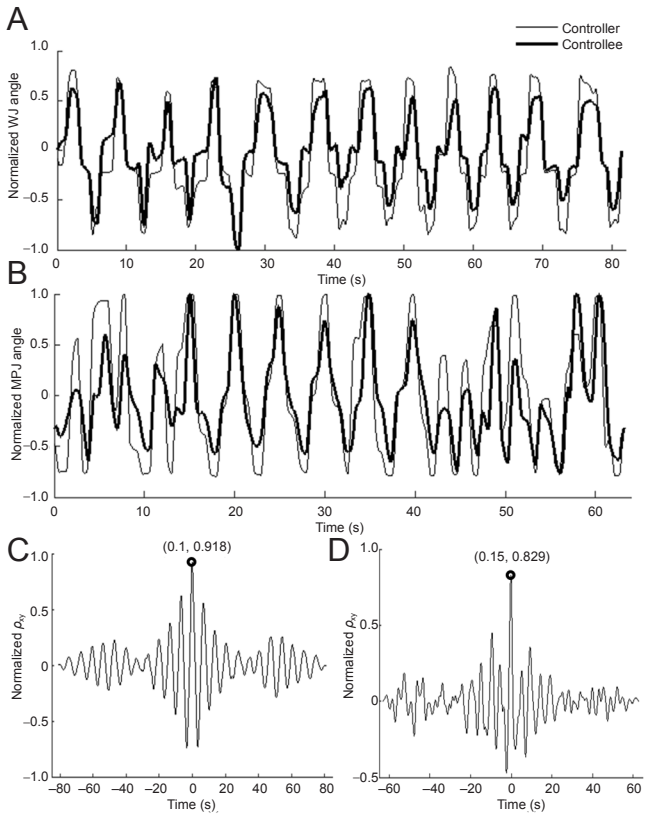


**Figure 8 Representative results of the joint angles in the real-time bridging test using the wearable EMG-bridge system.**
(A, B) Normalized tracing trajectories of wrist joint (WJ) and mean metacarpal-phalangeal joint (MPJ) angles of the five fingers (5F-MPJ). The gray and black color curves represent the joint angle of the controller (subject B) and the controlled (subject A). (C) Normalized cross-correlation ($\rho_{xy}$) function results between two WJ trajectories from the controller and the controlled. (D) The normalized cross-correlation function results between the two 5F-MPJ trajectories from the controller and the controlled. s: Second.

control to improve voluntary participation of hemiplegic patients. Movement of the controller's hand can be regenerated on the hand under control with high accuracy and low latency. For future studies, the feasibility of wearable EMG-bridge systems should be tested on hemiplegic patients using a contralaterally controlled FES paradigm to establish volitional participation of paralyzed patients.

**Declaration of participant consent:** *The authors certify that they have*

*obtained all appropriate participant consent forms. In the form the participant(s) has/have given his/her/their consent for his/her/their images and other clinical information to be reported in the journal. The participants understand that their names and initials will not be published and due efforts will be made to conceal their identity, but anonymity cannot be guaranteed.*

**Acknowledgments:** *We would like to thank Chong-Yao Xu of Guangdong University of Science and Technology, China and Yu-Ting Su of Nanjing SQ Medical Device Corporation, China for their technical help.*

**Author contributions:** *HPW designed the study, manufactured the circuit, analyzed the data, and wrote the paper. ZYB and YZ designed and manufactured the circuits. YXZ performed the experiment and designed the motion assessment instruments. ZGW and XYL gave guidance to the design, developed the experimental method, and revised this paper. All authors approved the final version of the paper.*

**Conflicts of interest:** *None declared.*

**Plagiarism check:** *This paper was screened twice using CrossCheck to verify originality before publication.*

**Peer review:** *This paper was double-blinded and stringently reviewed by international expert reviewers.*

## References


Barsi GI, Popovic DB, Tarkka IM, Sinkjær T, Grey MJ (2008) Cortical excitability changes following grasping exercise augmented with electrical stimulation. Exp Brain Res 191:57-66.

Biering-Sørensen B, Kristensen IB, Kjaer M, Biering-Sørensen F (2009) Muscle after spinal cord injury. Muscle Nerve 40:499-519.

Binder-Macleod SA, McDermond LR (1992) Changes in the force-frequency relationship of the human quadriceps femoris muscle following electrically and voluntarily induced fatigue. Phys Ther 72:95-104.

Cauraugh JH, Kim SB, Duley A (2005) Coupled bilateral movements and active neuromuscular stimulation: intralimb transfer evidence during bimanual aiming. Neurosci Lett 382:39-44.

Cook AJ, Gargiulo GD, Lehmann T, Hamilton TJ (2015) Open platform, eight-channel, portable bio-potential and activity data logger for wearable medical device development. Electron Lett 51:1641-1643.

Craven BC, Hadi SC, Popovic MR (2015) Functional Electrical Stimulation Therapy: Enabling Function Through Reaching and Grasping. In: International Handbook of Occupational Therapy Interventions (Söderback I, ed), pp 587-605. Cham: Springer International Publishing.

Hafer-Macko CE, Ryan AS, Ivey FM, Macko RF (2008) Skeletal muscle changes after hemiparetic stroke and potential beneficial effects of exercise intervention strategies. J Rehabil Res Dev 45:261-272.

Hara Y, Obayashi S, Tsujiuchi K, Muraoka Y (2013) The effects of electromyography-controlled functional electrical stimulation on upper extremity function and cortical perfusion in stroke patients. Clin Neurophysiol 124:2008-2015.

Huang ZH, Wang ZG, Lv XY, Zhou YX, Wang HP, Zong SH (2014) A novel functional electrical stimulation-control system for restoring motor function of post-stroke hemiplegic patients. Neural Regen Res 9:2102-2110.

Ijzerman MJ, Stoffers TS, Klatte M, in't Groen FA, Snoek GJ, Vorsteveld JH, Nathan RH, Hermens HJ (1996) The NESS Handmaster orthosis: restoration of hand function in C5 and stroke patients by means of electrical stimulation. J Rehabil Sci 9:86-89.

Jiang N, Englehart KB, Parker PA (2009) Extracting simultaneous and proportional neural control information for multiple-DOF prostheses from the surface electromyographic signal. IEEE Trans Biomed Eng 56:1070-1080.

Jiang N, Rehbaum H, Vujaklija I, Graimann B, Farina D (2014) Intuitive, online, simultaneous, and proportional myoelectric control over two degrees-of-freedom in upper limb amputees. IEEE Trans Neural Syst Rehabil Eng 22:501-510.

Johnson LA, Fuglevand AJ (2011) Mimicking muscle activity with electrical stimulation. J Neural Eng 8:016009.

Kamen G, Du DC (1999) Independence of motor unit recruitment and rate modulation during precision force control. Neuroscience 88:643-653.

Kesar T, Chou LW, Binder-Macleod SA (2008) Effects of stimulation frequency versus pulse duration modulation on muscle fatigue. J Electromyogr Kinesiol 18:662-671.

Kilgore KL, Peckham PH, Keith MW, Thrope GB, Wuolle KS, Bryden AM, Hart RL (1997) An implanted upper-extremity neuroprosthesis. Follow-up of five patients. J Bone Joint Surg Am 79:533-541.

Knutson JS, Hisel TZ, Harley MY, Chae J (2009) A novel functional electrical stimulation treatment for recovery of hand function in hemiplegia: 12-week pilot study. Neurorehabil Neural Repair 23:17-25.

Knutson JS, Harley MY, Hisel TZ, Makowski NS, Chae J (2014) Contralaterally controlled functional electrical stimulation for recovery of elbow extension and hand opening after stroke: a pilot case series study. Am J Phys Med Rehabil 93:528-539.

Knutson JS, Harley MY, Hisel TZ, Hogan SD, Maloney MM, Chae J (2012) Contralaterally controlled functional electrical stimulation for upper extremity hemiplegia: an early-phase randomized clinical trial in subacute stroke patients. Neurorehabil Neural Repair 26:239-246.

Li G, Schultz AE, Kuiken TA (2010) Quantifying pattern recognition-based myoelectric control of multifunctional transradial prostheses. IEEE Trans Neural Syst Rehabil Eng 18:185-192.

Liberson WT, Holmquest HJ, Scot D, Dow M (1961) Functional electrotherapy: stimulation of the peroneal nerve synchronized with the swing phase of the gait of hemiplegic patients. Arch Phys Med Rehabil 42:101-105.

Lorrain T, Jiang N, Farina D (2011) Influence of the training set on the accuracy of surface EMG classification in dynamic contractions for the control of multifunction prostheses. J Neuroeng Rehabil 8:25.

Malešević NM, Maneski LZP, Ilić V, Jorgovanović N, Bijelić G, Keller T, Popović DB (2012) A multi-pad electrode based functional electrical stimulation system for restoration of grasp. J Neuroeng Rehabil 9:66.

McGie SC, Zariffa J, Popovic MR, Nagai MK (2015) Short-term neuroplastic effects of brain-controlled and muscle-controlled electrical stimulation. Neuromodulation 18:233-240.

Nathan RH (1989) An FNS-based system for generating upper limb function in the C4 quadriplegic. Med Biol Eng Comput 27:549-556.

Pfurtscheller G, Müller GR, Pfurtscheller J, Gerner HJ, Rupp R (2003) 'Thought'--control of functional electrical stimulation to restore hand grasp in a patient with tetraplegia. Neurosci Lett 351:33-36.

Phinyomark A, Phukpattaranont P, Limsakul C (2012) Feature reduction and selection for EMG signal classification. Expert Syst Appl 39:7420-7431.

Popović-Maneski L, Kostić M, Bijelić G, Keller T, Mitrović S, Konstantinović L, Popović DB (2013) Multi-pad electrode for effective grasping: design. IEEE Trans Neural Syst Rehabil Eng 21:648-654.

Popović DB (2014) Advances in functional electrical stimulation (FES). J Electromyogr Kinesiol 24:795-802.

Saxena S, Nikolić S, Popović D (1995) An EMG-controlled grasping system for tetraplegics. J Rehabil Res Dev 32:17-24.

Shen XY, Du W, Huang W, Chen Y (2016) Rebuilding motor function of the spinal cord based on functional electrical stimulation. Neural Regen Res 11:1327-1332.

Thorsen R, Spadone R, Ferrarin M (2001) A pilot study of myoelectrically controlled FES of upper extremity. IEEE Trans Neural Syst Rehabil Eng 9:161-168.

Wang H, Wang ZG, Wang R, Xu J, Fan WN (2012) RF front-end for 315/433MHz super-regenerative receiver. Dianlu yu Xitong Xuebao 17:15-19.

Wade RC, Gorgey AS (2016) Skeletal muscle conditioning may be an effective rehabilitation intervention preceding functional electrical stimulation cycling. Neural Regen Res 11:1232-1233.

Wang HP, Wang ZG, Lü XY, Huang ZH, Zhou YX (2015) Design of a pulse-triggered four-channel functional electrical stimulator using complementary current source and time division multiplexing output method. Conf Proc IEEE Eng Med Biol Soc 2015:1671-1674.

Zhou Y, X L, Wang Z, Huang Z, Yang J, Zhao X (2011) Surface myoelectric signals decoding using the continuous wavelet transform singularity detection. Bioelectronics and Bioinformatics (ISBB), 2011 International Symposium on 2011:191-194.

Zhou YX, Wang HP, Bao XL, Lü XY, Wang ZG (2016) A frequency and pulse-width co-modulation strategy for transcutaneous neuromuscular electrical stimulation based on sEMG time-domain features. J Neural Eng 13:016004.


*Copyedited by Cooper C, Robens J, Yu J, Qiu Y, Li CH, Song LP, Zhao M*